Machine learning enabled onsite electrochemical detection of lidocaine using a microneedle array integrated screen printed electrode

Sachin Kadian¹, Siba Sundar Sahoo³, Pratima Kumari² and Roger J. Narayan^{1,3}

¹Joint Department of Biomedical Engineering, University of North Carolina and North Carolina State University, Raleigh, NC 27695, USA

²University of California San Francisco, San Francisco, CA 94143, USA
³Department of Materials Science and Engineering, North Carolina State University, Raleigh, NC 27695, USA

Corresponding author: Roger Narayan, Joint Department of Biomedical Engineering, University of North Carolina and North Carolina State University, Raleigh, NC 27695, USA, rjnaraya@ncsu.edu

First author email address: skadian@ncsu.edu

Abstract

Despite several advantageous uses of lidocaine patches to overcome discomfort and pain in various clinical settings, overdosage of this drug can cause unwanted side effects on the cardiovascular and central nervous system, which can lead to life-threatening conditions. Therefore, the development of a rapid, sensitive, and user-friendly point-of-care device for onsite lidocaine detection is of great clinical importance. To address this issue, we have developed a machine learning enabled wireless microneedle array integrated screen-printed electrode-based electrochemical point-of-care device for rapid and effective detection of lidocaine. The fabricated device utilizes novel ultra-sharp microneedles arrays having a reservoir in its base, which are designed to collect the interstitial fluid through open side channels, and graphene-modified screen-printed carbon electrodes for the electrochemical detection of lidocaine. Under optimal conditions, the developed sensor exhibited high sensitivity and good selectivity towards lidocaine along with a linear current response over the detection range from 1-120 μ M with the lowest detection limit of 0.13 μ M. In addition, to make the device user friendly, a machine learning model was developed using experimental sensing data to predict the lidocaine concentration and further deployed to prepare a web application for digital visualization of lidocaine concentration.

Keywords: graphene; screen printing; microneedle; lidocaine; biosensing

1. Introduction

Lidocaine (2-(diethylamino)-N-(2,6-dimethylphenyl) acetamide hydrochloride monohydrate) is an amide prepared from cocaine [1]. It is effective in reducing acute and chronic pain related to medical procedures, including gynecological, dental, and surgical procedures; this local anesthetic and peripheral analgesic compound is administered intravenously, topically, epidurally, or subcutaneously [2–4]. Along with that, lidocaine is also being used as an antiarrhythmic medicine; it is also sometimes unlawfully incorporated into cosmetic products to lower skin damage caused by sunlight exposure[5–9]. Further, topical lidocaine patches are often recommended to overcome the discomfort and pain triggered by muscle soreness, shingles, skin irritations, and hemorrhoid-related rectal uneasiness [10,11]. However, an overdosage of lidocaine can cause unwanted serious side effects on the central nervous system and cardiovascular system, such as low blood pressure, seizures, an irregular heart rate, and severe inflammatory responses [12,13]. Therefore, a precise, rapid, sensitive, and user-friendly point-of-care device for onsite lidocaine detection is needed to avoid overdosage-related complications.

Until this time, a few traditional methods such as high-performance liquid chromatography (HPLC), surface enhanced Raman scattering, gas chromatography-mass spectrometry (GC-MS), and optical methods (e.g., immunoassay and photoluminescence methods) have been used for the detection of lidocaine and other analytes [14-20]. Although these techniques can measure lidocaine, they often need complex pretreatments, expensive equipment, environmentally unfriendly reagents, and long working times with skilled operators, which limits their feasibility for rapid and onsite monitoring applications [21–25]. In addition, these approaches are highly vulnerable to false positive results due to poor sampling, improper handling, or pretreatments [26]. Recently, due to straightforward operation, a low detection limit, a low detection time, high sensitivity, and high specificity, the development of low-cost electrochemical sensing platforms for *in vitro* monitoring of various chemicals, including lidocaine, has gained significant attention from the pharmaceutical industry and the scientific community [27–34]. For instance, Yang et al. developed dendritic Pt-Pd bimetallic nanoparticles and a porous Pt nano-network-based electrochemical sensing platform for lidocaine detection [35]. Pinar et al. used an anodically pretreated boron-doped diamond electrode for the electrochemical detection of lidocaine over the 0.1-20.0 µmol L⁻¹ range [1]. Similarly, Oliveira et al. developed an electroanalytical method for the determination of lidocaine in a local anesthetic product using boron-doped diamond electrodes [21]. Saad et al. introduced a voltammetric method for the determination of lidocaine hydrochloride through the use of an electrochemically active C18 silica-modified carbon paste electrode [36]. Likewise, Rahbar et al. used a carbon paste electrode for the electrochemical detection of lidocaine [37]. Zhang et al. used an isoreticular metal-organic framework-8 derived porous carbon decorated glassy carbon electrode for the highly sensitive electrochemical detection of lidocaine [38]. Despite the noteworthy progress in the development of electrochemical biosensors, these methods rely on blood sample collection, finger pricking, and the use of nanomaterial electrode surface modification procedures; as such, they are unable to monitor the lidocaine concentration in physiologically relevant fluids in a straightforward manner [39–42]. Therefore, the fabrication of a wearable, user-friendly, minimally invasive electrochemical sensing platform that can overcome the above-mentioned issues by monitoring lidocaine concentration in interstitial fluid with high specificity is desirable.

Wearable sensor technology offers tremendous opportunities for the fabrication of various customized healthcare devices [43,44]. Among the many wearable sensing platforms developed in recent years, microneedle-based sensing systems have received significant consideration for use in straightforward, rapid, economical, minimally invasive, and continuous transdermal detection of numerous biomolecules in interstitial fluid [45–48]. Microneedles are economical micrometer-size devices that can create artificial pores in the skin via disruption of the stratum corneum layer of the epidermis; these devices are able to access interstitial fluid with minimal discomfort, pain, and tissue damage [49–54]. Due to its advantageous features, microneedle array-based sensing platforms have been used for the real-time determination of clinically important biomolecules, including organophosphate, glucose, alcohol, lactate, L dopa, and potassium ions [44,45,50,55,56]. To the best of our knowledge, no prior work has been reported for the fabrication of a microneedle array integrated sensing platform for onsite detection of lidocaine in interstitial fluid.

In this work, we have developed for the first time a machine learning enabled wireless microneedle array integrated screen-printed electrode-based electrochemical point-of-care device for rapid and effective detection of lidocaine. The developed microneedle integrated sensor takes advantage of 3D printing, microneedle technology, screen-printed electrodes, a paper-based microfluidic channel, and a capillarity system for straightforward fabrication of a microneedle array based

electrochemical point-of-care device. The fabricated sensor utilizes the novel ultra-sharp microneedle array that contains a reservoir at their base; these devices are designed to collect interstitial fluid through open side channels. Under optimal conditions, the developed wireless sensing platform exhibited high sensitivity and selectivity towards lidocaine along with a linear current response. Moreover, a machine learning model was developed using the obtained experimental sensing data to predict the lidocaine concentration and further deployed to prepare a web application for digital visualization of the lidocaine concentration to make the device user-friendly for onsite lidocaine detection. The obtained results demonstrated that by coupling a reservoir-fitted microneedle array with a paper-based microfluidic channel and capillarity system as well as a screen-printed electrode, a simple, user-friendly, and minimally invasive electrochemical sensing platform could be developed for onsite detection of lidocaine in the interstitial fluid. The fabrication of a novel reservoir-fitted microneedle array design and its integration with a screen-printed electrode as proposed in this study can potentially be explored for the development of various electrochemical sensors for onsite detection of other biomarkers in interstitial fluid.

2. Experimental section

2.1 Materials and Methods

Graphene-modified screen-printed carbon electrodes (L 33 mm x W 10 mm x H 0.5 mm) used in this study were obtained from Metrohm Dropsens - Oviedo (Asturias) Spain. All of the chemicals, including theophylline, caffeine, ascorbic acid, acetaminophen, cyclodextrin, uric acid, potassium ferricyanide, phosphate buffer, and ethanol, were purchased from Sigma-Aldrich, St. Louis, MO, USA. All of the other reagents were of analytical grade and used without any modifications. All stock solutions, dilutions, and samples were prepared in fresh deionized (DI) water, which was obtained from a Milli Q system (18.2 M Ω · cm at 25 °C) (Evoqua Water Technologies LLC, Chicago, IL, USA).

2.2 Microneedle design and fabrication

The ultra-sharp and high resolution $(2\mu m\sim 50\mu m)$ microneedle array used in this study was fabricated using Projection Micro Stereolithography (P μ SL) technology with an S130 3D-printer from Boston Micro Fabrication (BMF), Maynard, MA, USA. The microneedle array structure with

two conical shape needles, which exhibited a height of 1500 µm, a diameter of 500 µm, side channels facing each other, and a base diameter of 0.1 mm ending in a reservoir of diameter 0.4 mm, was designed with SolidWorks 2016 software (Dassault Systems, Vélizy-Villacoublay, France). The design was transferred to the BMF Slicer software for parameter setup and "slicing" into layers in order to generate the interpreted general writing language code for use in 3D printing. A yellow color biocompatible and transparent resin named photoreactive resin BIO, which contained a mixture of two methacrylate oligomers, lauryl methacrylate reactive diluent and diphenyl (2,4,6-trimethylbenzoyl) phosphine oxide photoinitiator, was obtained from BMF; this resin was used for microneedle array fabrication. A skin irritation, acute systemic toxicity, and in vitro cytotoxicity study of the resin was previously assessed by the manufacturer under the ISO 10 993-10: 2010, ISO 10 993-12: 2012, and ISO10 993-2: 2006 skin irritation test, the ISO 10 993-12: 2012 acute systemic toxicity test, and the ISO 10 993-12: 2012 in vitro cytotoxicity test. Upon completion of the printing process, the 3D-printed part was rinsed thrice in isopropyl alcohol to remove the traces of uncured resin from the open side channel and reservoir. After that, the resultant 3D-printed part was subjected to a post-curing process for 10 min at 45°C using a 405 nm wavelength lamp (Formlabs Inc., MA, USA).

2.3 Physical and electrochemical characterization

The surface morphology and structural dimensions of 3D-printed microneedle array were assessed using a variable pressure scanning electron microscope (VPSEM) Hitachi SU3900 (Tokyo, Japan), which was equipped with various detectors such as a standard Everhard-Thornley secondary electron detector, a five-segment solid state backscattered electron detector, and an accelerating voltage range from 0.3 to 30 kV. All of the electrochemical characterization of the screen-printed electrode-based electrochemical device, including stability, sensing, and selectivity experiments, were performed at room temperature using a PalmSens4 hand-held potentiostat (PalmSens BV, Utrecht, the Netherlands) powered by a rechargeable battery. All experiments were performed wirelessly; the measurements were sent to a personal computer (readout device) through wireless communications for further analysis.

2.4 Skin penetration and mechanical strength test

The skin penetration test of our 3D-printed microneedle array was investigated *ex vivo* using a porcine skin patch [51,56,57]. For this study, the fresh porcine skin was purchased from a local

supermarket and cleaned with an alcohol swab. Next, the wiped porcine skin was fixed on a board and manually punctured with our 3D-printed microneedle array. To show the skin penetration characteristics associated with the microneedle array, 0.4% Trypan Blue solution was applied to the microneedle array for better visualization of the pores using an optical microscope. Further, a Ubi-1 nanoindenter (Hysitron, Minneapolis, USA) was operated with a loading time of 20 s, maximum force of $1000~\mu N$, dwell time of 10~s, unloading time of 20~s, and a Berkovich-type tip was used to calculate the hardness and Young's modulus values of the microneedle material.

2.5 Fluid extraction test

Fluid extraction characterization of the 3D-printed microneedle array was performed by dipping the microneedle array into a diluted Trypan Blue solution. To accomplish this step, the cap of a small plastic box equipped with a manually created circular hole of 8 mm diameter was placed in a small Petri dish. Next, the plastic box-capped Petri dish was filled with Trypan Blue solution while ensuring no overflow of the solution. The 3D-printed microneedle array was then placed onto the manually created circular hole so that the microneedle tips were able to contact the solution. The functionality of the capillarity system provided by open-side channels was examined by placing blank paper on the upper surface of the 3D-printed microneedle array. The optical images of the fluid extraction experiments were captured using an iPhone 13 device (Cupertino, CA, USA).

2.6 Lidocaine detection and sample preparation

Before integrating the graphene-modified screen-printed carbon electrodes with the microneedle array and utilizing it for lidocaine detection, the electron transfer characteristics of the screen-printed electrode were investigated via the cyclic voltammetry response in a freshly prepared a 5 mM ferricyanide solution at a fixed scan rate of 50 mV/s. Next, the analytical performance of the fully integrated device towards lidocaine was examined by recording the square wave voltammetry response (at a frequency of 10 Hz and a potential range from 0.4 to 1.1 V) in freshly prepared phosphate buffered saline (PBS) electrolyte solution (0.1 M, pH 8) before and after spiking various concentrations of lidocaine. To prepare the sensing samples with a varying concentration of lidocaine, a freshly prepared stock solution (1.0 mg/mL) of lidocaine in ethanol was diluted with PBS.

2.7 Proof-of-concept study

In order to examine the real-time application of the fully integrated lidocaine sensing device, the electrochemical performance of the device was further examined by recording the square wave voltammetry response in artificial interstitial fluid while penetrating the skin-mimicking parafilm layer. For this, the artificial interstitial fluid with varying concentrations of lidocaine was filled in a Petri dish and carefully sealed with a parafilm layer. To initiate testing, a wireless microneedle array integrated sensing device was gently pressed so that the microneedle tips were able to penetrate the skin-mimicking parafilm layer and contact the solution. After a few seconds, the square wave voltammetry response was recorded at a frequency of 10 Hz over a potential range from 0.4 to 1.1 V and a potential step of 0.01 V.

2.8 Machine learning model and user interface

Machine learning is an automated data analysis approach for decision making that does not rely on any explicit instruction and is currently being integrated with healthcare devices as well for the onsite detection of the various analytes [58–61]. The algorithms "learn" the decision rule from the input data and utilize it to make further predictions [62–64]. In this study, a machine learning-based regression algorithm was used to build a predictive model, which was trained on a dataset that consists of both input and output data. Regression is a modeling technique that is used to determine the relationship between the dependent variable (output) and the independent variable (input) [24,65,66]. This defined relationship is further used to predict or estimate the value of the output variable based on the value of the given input variable. Since the data in this study follows a linear trend and has a single independent variable, a univariate linear regression model was trained on the obtained experimental data of square wave voltammetry to predict the lidocaine concentration. Univariate linear regression can be defined as a regression modeling technique that models the relationship between a single dependent variable and a single independent variable [67–71]. Simple univariate linear regression can be mathematically demonstrated as follows:

$$\hat{y} = \beta_0 + \beta_1 x$$

In this equation, \hat{y} is the predicted output, $\beta_0 + \beta_1 x$ represents the straight line that fits the data, and x is the value of the input variable; β_0 and β_1 are the intercept and slope of the straight line, respectively. The goal is to determine the most optimized values of β_0 and β_1 using the least squares

method. The least square method attempted to minimize the average of the squared difference between the actual and predicted value of output in order to identify the best fit line/function. Further, the performance of the trained linear regression model was evaluated using two metrics, namely Mean square error (MSE) and Coefficient of Determination (R²). MSE is a statistical metric that measures the average squared difference between the actual and predicted value of output in a regression model. It can be mathematically represented as follows:

$$MSE = \frac{1}{n}(y - \hat{y})^2$$

In this equation, n is the number of data points, y is the actual value of output and \hat{y} is the predicted value of output. A lower value of MSE means a better regression model. R^2 is a statistical metric used to evaluate the goodness-of-fit of a linear regression model, which represents the proportion of the variance in the output variable that can be explained by the input variable. It measures how well the linear regression model fits the actual data points and shows the agreement between actual and predicted values of output. It can be mathematically represented as follows:

$$R^2 = 1 - \frac{SSR}{SST}$$

In this equation, SSR is the Sum of Squared Residuals, which was calculated as the sum of the squared differences between the predicted values and actual values of the output variable. SST is the total Sum of Squares, which was calculated as the sum of the squared differences between the actual values and the mean of the output variable. The R^2 ranges from 0 to 1, where a higher value represents better performance of the model.

In this work, the experimental dataset contains the peak current value obtained from the square wave voltammetry spectra and the corresponding lidocaine concentration value. Thus, the univariate linear regression was employed to train the model while utilizing the peak current value as the input value and the lidocaine concentration as the output variable. A least square loss function was utilized to determine the optimal values of the coefficients and establish a linear regression equation. Once the model was developed, it was further utilized to predict the lidocaine concentration. Finally, for better human interaction and usability, the developed linear regression model was deployed as a web application to provide accessibility, real-time operation, and ease-of-use for end users to predict the lidocaine concentration. In order to integrate the trained

machine learning model into a web application, a popular Python web framework, namely Flask, Hyper Text Markup Language (HTML), and Cascading Style Sheets (CSS), was utilized. Flask is an open-source lightweight web framework that was built in Python for the deployment of web applications; it was utilized to interlink the back-end and front-end. HTML was used to create a form that takes input from the user, and CSS was utilized to provide some styling to the web page. Flask received the input value through application programming interface (API) calls, computed the predicted value using the trained model, and returned it to the user.

3. Result and discussion

3.1 Design and integration of sensor

The proposed microneedle array integrated screen-printed electrode-based electrochemical point-of-care device (Figure 1) for rapid and effective detection of lidocaine consists of three components: (i) an ultra-sharp microneedles array, (ii) a paper microfluidics channel, and (iii) a screen-printed electrode. Figure 1a demonstrates the exploded view of different components and stepwise assembly process of the microneedle array integrated device. Figure 1b shows the schematic diagram of fully assembled device instead into skin layer. Since the hollow microneedles can become clogged during interstitial fluid sampling, the novel microneedle array used in this study was designed with open side channels (instead of a cavity at the center) along with a reservoir that was built into the base of microneedles. The reservoir was incorporated and designed between two microneedles having their open side channel facing each other to ensure the straightforward and uninterrupted collection of interstitial fluid for diagnosis. Such a design permits interstitial fluid to be drawn into the reservoir by capillary pressure via the shaft offered by open side channels of the microneedle. The microneedles were created to be long enough to ensure the appropriate skin penetration and avoid skin folding around the microneedle tip. Next, the paper microfluidics was sandwiched between the microneedle array reservoir and screen-printed electrode (Figure 1a) to ensure the efficient and autonomous transport of interstitial fluid from the reservoirs to the screen-printed electrode via a hydrophilic membrane and capillarity system. Further, the graphene-modified screen-printed carbon electrode was used for the electrochemical detection of lidocaine by means of a PalmSens4 hand-held potentiostat. Figure 1c displays the schematic of fully assembled device connected with wireless sensor. The obtained electrical signals were sent to the personal computer (readout device) via wireless communications

for further analysis through machine learning-enabled linear regression models (**figure 1d**). The machine learning model was successfully trained and tested on the as-obtained experimental sensing data; a program was developed for direct digital demonstration of the lidocaine concentration by simply entering the current value that was recorded by the potentiostat.

3.2 Fabrication and Characterization of Microneedle Array

The ultra-sharp microneedle array (**Figure 2a**) with open side channels and a reservoir in the base was designed using SolidWorks 2016 software. Since the microneedle array-based interstitial fluid collection and sensing strategies require a material with a high Young's modulus value that can easily penetrate the skin, a yellow color biocompatible and transparent resin named photoreactive resin BIO was used for the fabrication of the microneedle array. Under the 3D-printing digital light process, this resin allows for the fabrication of custom-designed micrometer-scale feature structures with easy removal of unpolymerized material. **Figure 2b** and **2c** demonstrate the macroscopic images of 3D-printed microneedle array. Further, in order to confirm the successful fabrication and obtain insight into the micrometer-scale features of open side channels and reservoir, SEM images of 3D-printed microneedle array were collected. **Figures 2d** and **2e** exhibit the characteristic topographic and sharpness features of the 3D-printed microneedle array at two different angles and magnifications. It can be observed from the SEM images that the open side channels were extended from the needle tip to the reservoir in a manner similar to the design shown in **Figure 2a**; this result confirms the successful fabrication of the designed microneedle array.

Since the skin penetration capability plays an important role in assessing the potential of the microneedle array design for use in interstitial fluid collection and sensing, the skin penetration ability of our 3D-printed microneedle array was assessed on a porcine skin patch, which biochemically and anatomically mimics human skin. **Figure 3a** shows the optical images of porcine skin punctured with a microneedle array before Trypan Blue staining; **Figures 3b & 3c** show optical images at two different magnifications of punctured skin after Trypan Blue treatment for better visualization of microneedle array-generated pores. It can be noticed from the figure that a confined penetration wound is created by each microneedle without any deformation or damage to the surrounding skin. Further, the mechanical properties of the microneedle material were examined using the nanoindentation technique. The Young's modulus and hardness values of the microneedle array material were measured to be 3.29 ± 0.12 GPa and 302.19 ± 10.44 MPa (mean

± standard deviation), respectively; the Young's modulus value is higher than the minimum Young's modulus value (1 GPa) required for human skin penetration [51]. Hence, these results indicate the skin penetration functionality of the 3D-printed microneedle array without any damage to the surrounding tissues; the results suggest that the microneedle array can be used for the development of an ISF sampling and sensing device.

3.3 Fluid extraction study

The autonomous fluid extraction functionality of the 3D-printed microneedle array plays a key role in further development of a sensing device. Therefore, the fluid extraction capability of 3D-printed microneedle array was investigated by inserting the UV-treated microneedle tip array into a diluted Trypan Blue solution. **Figure 4a** and **4b** display the complete experimental setup for the fluid extraction study (as discussed in Section 2). It was observed that the blue colored solution was readily drawn by microneedle tips upon initial contact with the liquid and transported to the reservoir due to surface tension via the open side channels. To confirm this process, a small piece of filter paper was placed (**Figure 4c**) on the upper surface of 3D-printed microneedle array; it was observed that the filter paper wicked (**Figure 4d**) the blue colored solution present in the microneedle reservoir via the capillarity system within a few seconds. In addition to the photographs shown in **Figure 4**, a short video (Supplementary Video 1) of the complete fluid extraction process was also recorded and included in the supplementary information. These results successfully demonstrate the fluid extraction capability of our 3D-printed microneedle array and indicate its potential for the development of an interstitial fluid sampling and sensing device.

3.4 Electrode stability and lidocaine sensing

After examining the skin penetration and fluid extraction potential of the 3D-printed microneedle array, the analytical performance of the fully integrated device towards lidocaine was assessed. However, prior to assembling the device, the electrochemical properties and stability of the graphene-modified screen-printed carbon electrode were investigated through the cyclic voltammetry technique. For this, the cyclic voltammetry response from the graphene-modified screen-printed carbon electrode was recorded in freshly prepared 5mM ferricyanide solution at a fixed scan rate of 50 mV/s and room temperature. The recorded cyclic voltammetry response demonstrated in **Figure 5a** showed a reversible redox behavior, revealing the efficient electrochemical charge transfer characteristics associated with the printed electrodes. Further,

because the stability of electrodes can impact the practical application of the device, the stability of the graphene-modified screen-printed carbon electrode was studied by recording the cyclic voltammetry response for five scans. It was observed (**Figure 5a**) that the cyclic voltammetry curves were well overlapped for all of the scans, indicating that the oxidation and reduction peak current remained the same for all the scans, thus suggesting th good stability of the printed electrodes.

Upon successful investigation of the electrochemical properties and stability of the graphene-modified screen-printed carbon electrode, the electrochemical sensing potential of graphene-modified screen-printed carbon electrode towards different concentrations (1-120 μ M) of lidocaine was studied through the square wave voltammetry technique. The obtained current signals against varying concentrations of lidocaine at a frequency, an amplitude and voltage step of 10 Hz, 0.1 V and 0.01 V, respectively, are shown in **Figure 5b**. It can be noted from the square wave voltammetry response that the peak current gradually increased with an increasing concentration of lidocaine. Next, the obtained peak current values were plotted against different concentrations of lidocaine as shown in **Figure 5c**. A linear relationship between the lidocaine concentration and peak current was observed over the range from 1 to 120 μ M with an R^2 value of 0.9817. The limit of detection was calculated using the equation 3s/M, where s is the standard error and s is the slope of the linear curve; it is measured to be as low as 0.13 μ M. Further, the sensitivity of the lidocaine sensor was also evaluated through the slope of the linear plot and found to be 0.83 μ A μ M⁻¹. As a result, the values of these analytical parameters, including the dynamic range, detection limit, and sensitivity, are sufficient for lidocaine sensing.

3.5 Selectivity assay

While the developed lidocaine sensing platform demonstrated excellent analytical performance, the selectivity towards lidocaine also plays a crucial role in evaluating the effectiveness of the electrochemical sensor. Thus, the selectivity of the lidocaine sensing platform was investigated by assessing the variation in current response in the presence of different interfering analytes, including theophylline, caffeine, ascorbic acid, acetaminophen, cyclodextrin, and uric acid. In this analysis, the square wave voltammetry response for each interfering analyte was recorded by spiking the same concentration (40 μ M) in freshly prepared samples, while maintaining all the other parameters constant. The square wave voltammetry spectra shown in **Figure 6** demonstrated

a selective square wave voltammetry response in the presence of different interfering analytes without an overlap with the lidocaine spectra. Therefore, these results enable us to conclude that the developed lidocaine sensing platform is selective to lidocaine.

3.6 Proof-of-concept demonstration of integrated device

After realizing the favorable analytical performance of the graphene-modified screen-printed carbon electrode towards lidocaine, the 3D-printed microneedle array integrated screen-printed electrode-based electrochemical point-of-care device was assembled using the steps shown in Figure 1a. Figure 7a and 7b show the realistic images of the fully assembled device. To further evaluate the functionality and effectiveness of the integrated device in a real-time scenario, the analytical performance of the device was further assessed by recording the square wave voltammetry response in artificial interstitial fluid while penetrating the skin-mimicking parafilm layer. Figure 7c and 7d depict the schematic diagram and photograph of the experimental setup used for the proof-of-concept demonstration, respectively. In this approach, six different concentrations (10-100 µM) of lidocaine were spiked in the artificial interstitial fluid; their respective square wave voltammetry response was recorded at a frequency of 10 Hz over a potential range from 0.4 to 1.1 V. The obtained current response shown in **Figure 7e** clearly reveals a systematic change in the peak current with an increasing concentration of lidocaine. For further quantitative analysis, these corresponding current values were plotted against the spiked concentrations of lidocaine; it was observed that the calibration curve (Figure 7f) showed good linearity and high sensitivity for lidocaine. Further, the reproducibility of the microneedle array-based sensing platform was evaluated by assembling multiple devices under similar circumstances; the obtained analytical performance was found to be comparable with an RSD of 2.65%. Therefore, these results affirm that the proposed 3D-printed microneedle array-based sensing platform is capable of detecting micromolar concentrations of lidocaine in the artificial interstitial fluid.

3.7 Machine learning enabled lidocaine detection and digital visualization

Further, in order to make the device user-friendly for onsite lidocaine detection, a machine learning model was developed and deployed to prepare a web application for digital visualization of the lidocaine concentration. For this, a univariate linear regression model was built using the obtained experimental sensing data to predict the lidocaine concentration. To find the best-fit line of

regression, the model was trained by minimizing the least squares cost function to determine the optimal value of coefficients. As a result, the best-fit line obtained from the developed linear regression model fits the experimental data points very well (as shown in **Figure 8a**). The optimal value of β_0 and β_1 were measured to be -161.1985 and 0.8208, respectively; thus, the equation of regression becomes $\hat{y} = -161.1985 + 0.8208x$, in which \hat{y} and x represent the predicted lidocaine concentration and input peak current values, respectively. It was observed that the developed regression model showed good performance with an R^2 value of 0.98, which was shown to be in good agreement with the experimental results.

Furthermore, the developed linear regression model was deployed as a web application to provide accessibility and ease-of-use for end users through the digital visualization of the lidocaine concentration. In this approach, a web application was developed, which requests the user to enter the peak current value obtained from the square wave voltammetry response as shown in **Figure 8b**. As soon as the user provides the input and presses the predict button, the flask makes the API calls and instantiates the developed linear regression model to perform the calculations in the back end. As a result, the machine learning model predicts the lidocaine concentration and displays the same on the web page as shown in **Figure 8c-8g**. In order to validate the effectiveness of the machine learning model and developed user interface, the lidocaine concentration was predicted multiple times (**Figure 8c-8g**) and compared with the experimental results. It was observed that the lidocaine concentration predicted through the machine learning model was in good agreement with the experimental results. Therefore, these results enable us to conclude that the developed machine model and user interface can readily be used for onsite detection of micromolar concentrations of lidocaine; this approach provides a user-friendly digital value of lidocaine concentration.

Conclusions

In this work, we have demonstrated a novel approach for machine learning enabled rapid and onsite detection of lidocaine in interstitial fluid using a 3D-printed microneedle array integrated screen-printed electrode-based electrochemical point-of-care device. The microneedle integrated sensor was fabricated using various additive manufacturing techniques, including a 3D-printing process, screen-printed electrodes, a paper-based microfluidic channel, and a capillarity system for the scalable and economical production of the device. The developed wireless sensing platform

demonstrated a low detection limit, high sensitivity, and excellent selectivity towards lidocaine in the presence of potential interfering agents along with a linear current response. In addition, the excellent lidocaine prediction performance of the developed machine learning model and its digital visualization through the user interface encourages the onsite and user-friendly detection of lidocaine. The obtained result suggests that such a novel approach can potentially be explored for the development of various electrochemical sensors for the onsite detection of other biomarkers in interstitial fluid.

Conflict of interest

There are no financial or personal conflicts to declare for the work reported in this paper.

Acknowledgments

The authors wish to acknowledge support from National Science Foundation Award Number 2029974. This work was performed in part at the Analytical Instrumentation Facility (AIF) at North Carolina State University, which is supported by the State of North Carolina and the National Science Foundation (award number ECCS-2025064). The AIF is a member of the North Carolina Research Triangle Nanotechnology Network (RTNN), a site in the National Nanotechnology Coordinated Infrastructure (NNCI).

References

- [1] P.T. Pınar, Y. Yardım, Z. Şentürk, İndividual and simultaneous electroanalytical sensing of epinephrine and lidocaine using an anodically pretreated boron-doped diamond electrode by square-wave voltammetry, Diam Relat Mater. 101 (2020). https://doi.org/10.1016/j.diamond.2019.107649.
- [2] E. Marret, M. Rolin, M. Beaussier, F. Bonnet, Meta-analysis of intravenous lidocaine and postoperative recovery after abdominal surgery, in: British Journal of Surgery, 2008. https://doi.org/10.1002/bjs.6375.
- [3] A. Krishnakumar, R.K. Mishra, S. Kadian, A. Zareei, U.H. Rivera, R. Rahimi, Printed graphene-based electrochemical sensor with integrated paper microfluidics for rapid lidocaine detection in blood, Anal Chim Acta. 1229 (2022) 340332. https://doi.org/10.1016/J.ACA.2022.340332.
- [4] M. Guney, B. Oral, G. Bayhan, T. Mungan, Intrauterine lidocaine infusion for pain relief during saline solution infusion sonohysterography: A randomized, controlled trial, J Minim Invasive Gynecol. 14 (2007). https://doi.org/10.1016/j.jmig.2007.02.007.
- [5] J.J. Adcock, G.J. Douglas, M. Garabette, M. Gascoigne, G. Beatch, M. Walker, C.P. Page, RSD931, a novel anti-tussive agent acting on airway sensory nerves, Br J Pharmacol. 138 (2003). https://doi.org/10.1038/sj.bjp.0705056.
- [6] A. Krishnakumar, S. Kadian, U. Heredia Rivera, S. Chittiboyina, S.A. Lelièvre, R. Rahimi, Organ-on-a-Chip Platform with an Integrated Screen-Printed Electrode Array for Real-Time Monitoring Trans-Epithelial Barrier and Bubble Formation, ACS Biomater Sci Eng. (2022). https://doi.org/10.1021/acsbiomaterials.2c00494.
- [7] R. Porrà, S. Berri, L. Gagliardi, P. Chimenti, A. Granese, D. De Orsi, I. Carpani, D. Tonelli, Development of an HPLC method for the identification and dosage of non-allowed substances in cosmetic products. Part I: Local anaesthetics and antihistaminics, Anal Bioanal Chem. 380 (2004). https://doi.org/10.1007/s00216-004-2807-7.
- [8] S. Kadian, A. Kalkal, V. Jain, S. Shukla, R.J. Narayan, Pomegranate leaf extract-based carbon dots for the selective detection of 2,4,6-trinitrophenol, MRS Commun. (2023). https://doi.org/10.1557/s43579-023-00430-6.
- [9] S. Kadian, G. Manik, N. Das, P. Nehra, R.P. Chauhan, P. Roy, Synthesis, characterization and investigation of synergistic antibacterial activity and cell viability of silver-sulfur doped graphene quantum dot (Ag@S-GQDs) nanocomposites, J Mater Chem B. 8 (2020). https://doi.org/10.1039/c9tb02823d.
- [10] J. Kestřánek, Hemorrhoid management in women: The role of tribenoside + lidocaine, Drugs Context. 8 (2019). https://doi.org/10.7573/dic.212602.
- [11] R.W. Johnson, T.L. Whitton, Management of herpes zoster (shingles) and postherpetic neuralgia, Expert Opin Pharmacother. 5 (2004). https://doi.org/10.1517/14656566.5.3.551.
- [12] R.E. Johnstone, M.K. Wax, D.J. Bishop, J.B. Chafin, Large doses of topical lidocaine during microvascular surgery are not associated with toxic blood concentrations, Anesthesiology. 82 (1995). https://doi.org/10.1097/00000542-199502000-00034.

- [13] P.C. Pandey, M.D. Mitra, S. Shukla, R.J. Narayan, Organotrialkoxysilane-functionalized noble metal monometallic, bimetallic, and trimetallic nanoparticle mediated non-enzymatic sensing of glucose by resonance rayleigh scattering, Biosensors (Basel). 11 (2021). https://doi.org/10.3390/bios11040122.
- [14] E. Ricci, M.V.L.B. Bentley, J. Maldonado Marchetti, HPLC assay of lidocaine in in vitro dissolution test of the poloxamer 407 gels, Revista Brasileira de Ciencias Farmaceuticas/Brazilian Journal of Pharmaceutical Sciences. 38 (2002). https://doi.org/10.1590/s1516-93322002000100011.
- [15] S. Kadian, G. Manik, Sulfur doped graphene quantum dots as a potential sensitive fluorescent probe for the detection of quercetin, Food Chem. 317 (2020). https://doi.org/10.1016/j.foodchem.2020.126457.
- [16] S. Kadian, G. Manik, A highly sensitive and selective detection of picric acid using fluorescent sulfur-doped graphene quantum dots, Luminescence. 35 (2020). https://doi.org/10.1002/bio.3782.
- [17] F.O. Chagas, M.C. Hespanhol, L.H.M. Da Silva, P.R. Patrício, A.O. Maldaner, T.S. Soares, A.S.B. Castro, P.A. Marinho, An optical sensor for the detection and quantification of lidocaine in cocaine samples, Analyst. 145 (2020). https://doi.org/10.1039/d0an01246g.
- [18] F. Plössl, M. Giera, F. Bracher, Multiresidue analytical method using dispersive solid-phase extraction and gas chromatography/ion trap mass spectrometry to determine pharmaceuticals in whole blood, J Chromatogr A. 1135 (2006). https://doi.org/10.1016/j.chroma.2006.09.033.
- [19] A. Kalkal, S. Kadian, R. Pradhan, G. Manik, G. Packirisamy, Recent advances in graphene quantum dot-based optical and electrochemical (bio)analytical sensors, Mater. Adv. 2 (2021) 5513–5541. https://doi.org/10.1039/D1MA00251A.
- [20] A. Kalkal, S. Kadian, S. Kumar, G. Manik, P. Sen, S. Kumar, G. Packirisamy, Ti3C2-MXene decorated with nanostructured silver as a dual-energy acceptor for the fluorometric neuron specific enolase detection, Biosens Bioelectron. 195 (2022). https://doi.org/10.1016/j.bios.2021.113620.
- [21] R.T.S. Oliveira, G.R. Salazar-Banda, V.S. Ferreira, S.C. Oliveira, L.A. Avaca, Electroanalytical determination of lidocaine in pharmaceutical preparations using boron-doped diamond electrodes, Electroanalysis. 19 (2007). https://doi.org/10.1002/elan.200603840.
- [22] S. Kadian, S.K. Sethi, G. Manik, Recent advancements in synthesis and property control of graphene quantum dots for biomedical and optoelectronic applications, Mater Chem Front. 5 (2021). https://doi.org/10.1039/d0qm00550a.
- [23] R. Kumar, J. Kumar, S. Kadian, P. Srivastava, G. Manik, M. Bag, Tunable ionic conductivity and photoluminescence in quasi-2D CH3NH3PbBr3 thin films incorporating sulphur doped graphene quantum dots, Phys. Chem. Chem. Phys. 23 (2021) 22733–22742. https://doi.org/10.1039/D1CP03621A.
- [24] P. Kumari, D. Toshniwal, Deep learning models for solar irradiance forecasting: A comprehensive review, J Clean Prod. 318 (2021). https://doi.org/10.1016/j.jclepro.2021.128566.
- [25] P. Kumari, D. Toshniwal, Advanced machine learning techniques for short-term solar irradiance forecasting, in: Proceedings of the International Conference on AI-ML Systems (AI-ML Systems' 21). ACM, 2021: p. 4.

- [26] X. Xiong, Y. Li, W. Yuan, Y. Lu, X. Xiong, Y. Li, X. Chen, Y. Liu, Screen printed bipolar electrode for sensitive electrochemiluminescence detection of aflatoxin B1 in agricultural products, Biosens Bioelectron. 150 (2020). https://doi.org/10.1016/j.bios.2019.111873.
- [27] Z. Li, S. Kadian, R.K. Mishra, T. Huang, C. Zhou, S. Liu, Z. Wang, R. Narayan, Z. Zhu, Electrochemical detection of cholesterol in human biofluid using microneedle sensor, J Mater Chem B. (2023). https://doi.org/10.1039/D2TB02142K.
- [28] S. Kadian, B.D. Arya, S. Kumar, S.N. Sharma, R.P. Chauhan, A. Srivastava, P. Chandra, S.P. Singh, Synthesis and Application of PHT-TiO2 Nanohybrid for Amperometric Glucose Detection in Human Saliva Sample, Electroanalysis. 30 (2018). https://doi.org/10.1002/elan.201800207.
- [29] P.C. Pandey, H.P. Yadav, S. Shukla, R.J. Narayan, Electrochemical sensing and removal of cesium from water using prussian blue nanoparticle-modified screen-printed electrodes, Chemosensors. 9 (2021). https://doi.org/10.3390/chemosensors9090253.
- [30] P. Joshi, S. Shukla, S. Gupta, P.R. Riley, J. Narayan, R. Narayan, Excimer Laser Patterned Holey Graphene Oxide Films for Nonenzymatic Electrochemical Sensing, ACS Appl Mater Interfaces. 14 (2022). https://doi.org/10.1021/acsami.2c09096.
- [31] S. Kumar, J. Kumar, S.N. Sharma, Nanostructured titania based electrochemical impedimetric biosensor for non-invasive cancer detection, Mater Res Express. 5 (2018). https://doi.org/10.1088/2053-1591/aae1e2.
- [32] S. Kadian, N. Chaulagain, N.N. Joshi, K.M. Alam, K. Cui, K. Shankar, G. Manik, R.J. Narayan, Probe sonication-assisted rapid synthesis of highly fluorescent sulfur quantum dots, Nanotechnology. 34 (2023) 30LT01. https://doi.org/10.1088/1361-6528/acd00a.
- [33] S. Kadian, S. Shukla, R.J. Narayan, Probes for Noninvasive Biological Visualization and Biosensing of Cancer Cells, Appl Phys Rev. 10 (2023). https://doi.org/https://doi.org/10.1063/5.0166740.
- [34] T.A. Tabish, Y. Zhu, S. Shukla, S. Kadian, G.S. Sangha, C.A. Lygate, R.J. Narayan, Graphene nanocomposites for real-time electrochemical sensing of nitric oxide in biological systems, Appl Phys Rev. 10 (2023). https://doi.org/10.1063/5.0162640.
- [35] G. Yang, F. Zhao, A novel electrochemical sensor for the determination of lidocaine based on surface-imprinting on porous three-dimensional film, J Mater Chem C Mater. 2 (2014). https://doi.org/10.1039/c4tc02039a.
- [36] A.S. Saad, A.M.A. Al-Alamein, M.M. Galal, H.E. Zaazaa, Voltammetric Determination of Lidocaine and Its Toxic Metabolite in Pharmaceutical Formulation and Milk Using Carbon Paste Electrode Modified with C18 Silica, J Electrochem Soc. 166 (2019). https://doi.org/10.1149/2.0921902jes.
- [37] N. Rahbar, Z. Ramezani, A. Babapour, Electro-Oxidation Mechanism and Direct Square-Wave Voltammetric Determination of Lidocaine With a Carbon-Paste Electrode, Jundishapur J Nat Pharm Prod. 10 (2015). https://doi.org/10.17795/jjnpp-19382.
- [38] J. Zhang, J. Liu, Y. Zhang, F. Yu, F. Wang, Z. Peng, Y. Li, Voltammetric lidocaine sensor by using a glassy carbon electrode modified with porous carbon prepared from a MOF, and with a molecularly imprinted polymer, Microchimica Acta. 185 (2018). https://doi.org/10.1007/s00604-017-2551-2.

- [39] A. Kalkal, R. Pradhan, S. Kadian, G. Manik, G. Packirisamy, Biofunctionalized Graphene Quantum Dots Based Fluorescent Biosensor toward Efficient Detection of Small Cell Lung Cancer, ACS Appl Bio Mater. 3 (2020). https://doi.org/10.1021/acsabm.0c00427.
- [40] S. Kadian, G. Manik, A. Kalkal, M. Singh, R.P. Chauhan, Effect of sulfur doping on fluorescence and quantum yield of graphene quantum dots: An experimental and theoretical investigation, Nanotechnology. 30 (2019). https://doi.org/10.1088/1361-6528/ab3566.
- [41] S.K. Sethi, S. Kadian, G. Manik, A Review of Recent Progress in Molecular Dynamics and Coarse-Grain Simulations Assisted Understanding of Wettability, Archives of Computational Methods in Engineering. 29 (2022). https://doi.org/10.1007/s11831-021-09689-1.
- [42] S. Kadian, G. Manik, N. Das, P. Roy, Targeted bioimaging and sensing of folate receptor-positive cancer cells using folic acid-conjugated sulfur-doped graphene quantum dots, Microchimica Acta. 187 (2020). https://doi.org/10.1007/s00604-020-04448-8.
- [43] A.M.V. Mohan, J.R. Windmiller, R.K. Mishra, J. Wang, Continuous minimally-invasive alcohol monitoring using microneedle sensor arrays, Biosens Bioelectron. 91 (2017). https://doi.org/10.1016/j.bios.2017.01.016.
- [44] K.Y. Goud, C. Moonla, R.K. Mishra, C. Yu, R. Narayan, I. Litvan, J. Wang, Wearable Electrochemical Microneedle Sensor for Continuous Monitoring of Levodopa: Toward Parkinson Management, ACS Sens. 4 (2019). https://doi.org/10.1021/acssensors.9b01127.
- [45] R.K. Mishra, K.Y. Goud, Z. Li, C. Moonla, M.A. Mohamed, F. Tehrani, H. Teymourian, J. Wang, Continuous Opioid Monitoring along with Nerve Agents on a Wearable Microneedle Sensor Array, J Am Chem Soc. 142 (2020). https://doi.org/10.1021/jacs.0c01883.
- [46] H. Teymourian, F. Tehrani, K. Mahato, J. Wang, Lab under the Skin: Microneedle Based Wearable Devices, Adv Healthc Mater. 10 (2021). https://doi.org/10.1002/adhm.202002255.
- [47] S. Shukla, J. Jakowski, S. Kadian, R.J. Narayan, Computational approaches to delivery of anticancer drugs with multidimensional nanomaterials, Comput Struct Biotechnol J. 21 (2023) 4149–4158. https://doi.org/https://doi.org/10.1016/j.csbj.2023.08.010.
- [48] S.K. Sethi, S. Kadian, R. Gogoi, G. Manik, Layer-by-layer fabrication of self-cleaning superhydrophobic surface made from Carboxymethylcellulose and ZnO quantum dots: A combined experimental and computational study, Surfaces and Interfaces. 37 (2023). https://doi.org/10.1016/j.surfin.2023.102752.
- [49] P. Dardano, I. Rea, L. De Stefano, Microneedles-based electrochemical sensors: New tools for advanced biosensing, Curr Opin Electrochem. 17 (2019). https://doi.org/10.1016/j.coelec.2019.05.012.
- [50] Y. Zheng, R. Omar, R. Zhang, N. Tang, M. Khatib, Q. Xu, Y. Milyutin, W. Saliba, Y.Y. Broza, W. Wu, M. Yuan, H. Haick, A Wearable Microneedle-Based Extended Gate Transistor for Real-Time Detection of Sodium in Interstitial Fluids, Advanced Materials. 34 (2022). https://doi.org/10.1002/adma.202108607.
- [51] S.A. Machekposhti, S. Kadian, L. Vanderwal, S. Stafslien, R.J. Narayan, Novel hollow biodegradable microneedle for amphotericin B delivery, MedComm (Beijing). 4 (2023). https://doi.org/10.1002/mco2.321.

- [52] A. Zareei, V. Selvamani, S. Gopalakrishnan, S. Kadian, M.K. Maruthamuthu, Z. He, J. Nguyen, H. Wang, R. Rahimi, A Biodegradable Hybrid Micro/Nano Conductive Zinc Paste for Paper-Based Flexible Bioelectronics, Adv Mater Technol. 7 (2022). https://doi.org/10.1002/admt.202101722.
- [53] U. Heredia-Rivera, V. Kasi, A. Krishnakumar, S. Kadian, A.K. Barui, Z. He, H. Wang, L. Stanciu, R. Rahimi, Cold Atmospheric Plasma-Assisted Direct Deposition of Polypyrrole-Ag Nanocomposites for Flexible Electronic Sensors, ACS Appl Mater Interfaces. 15 (2023) 17078–17090. https://doi.org/10.1021/acsami.2c20798.
- [54] M. Chatterjee, P. Nath, S. Kadian, A. Kumar, V. Kumar, P. Roy, G. Manik, S. Satapathi, Highly sensitive and selective detection of dopamine with boron and sulfur co-doped graphene quantum dots, Sci Rep. 12 (2022). https://doi.org/10.1038/s41598-022-13016-4.
- [55] J. Kim, I. Jeerapan, J.R. Sempionatto, A. Barfidokht, R.K. Mishra, A.S. Campbell, L.J. Hubble, J. Wang, Wearable Bioelectronics: Enzyme-Based Body-Worn Electronic Devices, Acc Chem Res. 51 (2018). https://doi.org/10.1021/acs.accounts.8b00451.
- [56] S. Shukla, S.A. Machekposhti, N. Joshi, P. Joshi, R.J. Narayan, Microneedle-Integrated Device for Transdermal Sampling and Analyses of Targeted Biomarkers, Small Science. (2023). https://doi.org/10.1002/smsc.202200087.
- [57] S. Shukla, P. Joshi, P. Riley, R.J. Narayan, Square wave voltammetric approach to leptin immunosensing and optimization of driving parameters with chemometrics, Biosens Bioelectron. 216 (2022). https://doi.org/10.1016/j.bios.2022.114592.
- [58] P. Kumari, D. Toshniwal, Analysis of ANN-based daily global horizontal irradiance prediction models with different meteorological parameters: a case study of mountainous region of India, Int J Green Energy. 18 (2021). https://doi.org/10.1080/15435075.2021.1890085.
- [59] Y. Zhao, H. Zhang, Y. Li, X. Yu, Y. Cai, X. Sha, S. Wang, Z. Zhan, J. Xu, L. Liu, AI powered electrochemical multi-component detection of insulin and glucose in serum, Biosens Bioelectron. 186 (2021). https://doi.org/10.1016/j.bios.2021.113291.
- [60] S. Kadian, P. Kumari, S. Shukla, R. Narayan, Recent advancements in machine learning enabled portable and wearable biosensors, Talanta Open. 8 (2023) 100267. https://doi.org/10.1016/J.TALO.2023.100267.
- [61] S. Kadian, S. Shukla, R.J. Narayan, Probes for noninvasive biological visualization and biosensing of cancer cells, Appl Phys Rev. 10 (2023). https://doi.org/10.1063/5.0166740.
- [62] P. Kumari, D. Toshniwal, Impact of lockdown on air quality over major cities across the globe during COVID-19 pandemic, Urban Clim. 34 (2020). https://doi.org/10.1016/j.uclim.2020.100719.
- [63] P. Kumari, D. Toshniwal, Impact of lockdown measures during COVID-19 on air quality—A case study of India, Int J Environ Health Res. 32 (2022). https://doi.org/10.1080/09603123.2020.1778646.
- [64] P. Kumari, R. Wadhvani, Wind Power Prediction Using KLMS Algorithm, in: Proceedings of the International Conference on Inventive Research in Computing Applications, ICIRCA 2018, 2018. https://doi.org/10.1109/ICIRCA.2018.8597419.

- [65] P. Kumari, D. Toshniwal, HOURLY SOLAR IRRADIANCE PREDICTION FROM SATELLITE DATA USING LSTM, 2019.
- [66] V. Kammarchedu, D. Butler, A. Ebrahimi, A machine learning-based multimodal electrochemical analytical device based on eMoSx-LIG for multiplexed detection of tyrosine and uric acid in sweat and saliva, Anal Chim Acta. 1232 (2022). https://doi.org/10.1016/j.aca.2022.340447.
- [67] P. Kumari, D. Toshniwal, Long short term memory—convolutional neural network based deep hybrid approach for solar irradiance forecasting, Appl Energy. 295 (2021). https://doi.org/10.1016/j.apenergy.2021.117061.
- [68] P. Kumari, D. Toshniwal, Machine learning techniques for hourly global horizontal irradiance prediction: A case study for smart cities of India, in: International Conference on Applied Energy (ICAE), 2021: pp. 1–6.
- [69] P. Kumari, D. Toshniwal, Real-time estimation of COVID-19 cases using machine learning and mathematical models-The case of India, in: 2020 IEEE 15th International Conference on Industrial and Information Systems, ICIIS 2020 Proceedings, 2020. https://doi.org/10.1109/ICIIS51140.2020.9342735.
- [70] P. Kumari, D. Toshniwal, Extreme gradient boosting and deep neural network based ensemble learning approach to forecast hourly solar irradiance, J Clean Prod. 279 (2021). https://doi.org/10.1016/j.jclepro.2020.123285.
- [71] J. Watts, A. Potter, V. Mohan, P. Kumari, S.K. Thengane, S. Sokhansanj, Y. Cao, K.S. Kung, Proxy quality control of biomass particles using thermogravimetric analysis and Gaussian process regression models, Biofuels, Bioproducts and Biorefining. (2023).

List of figures

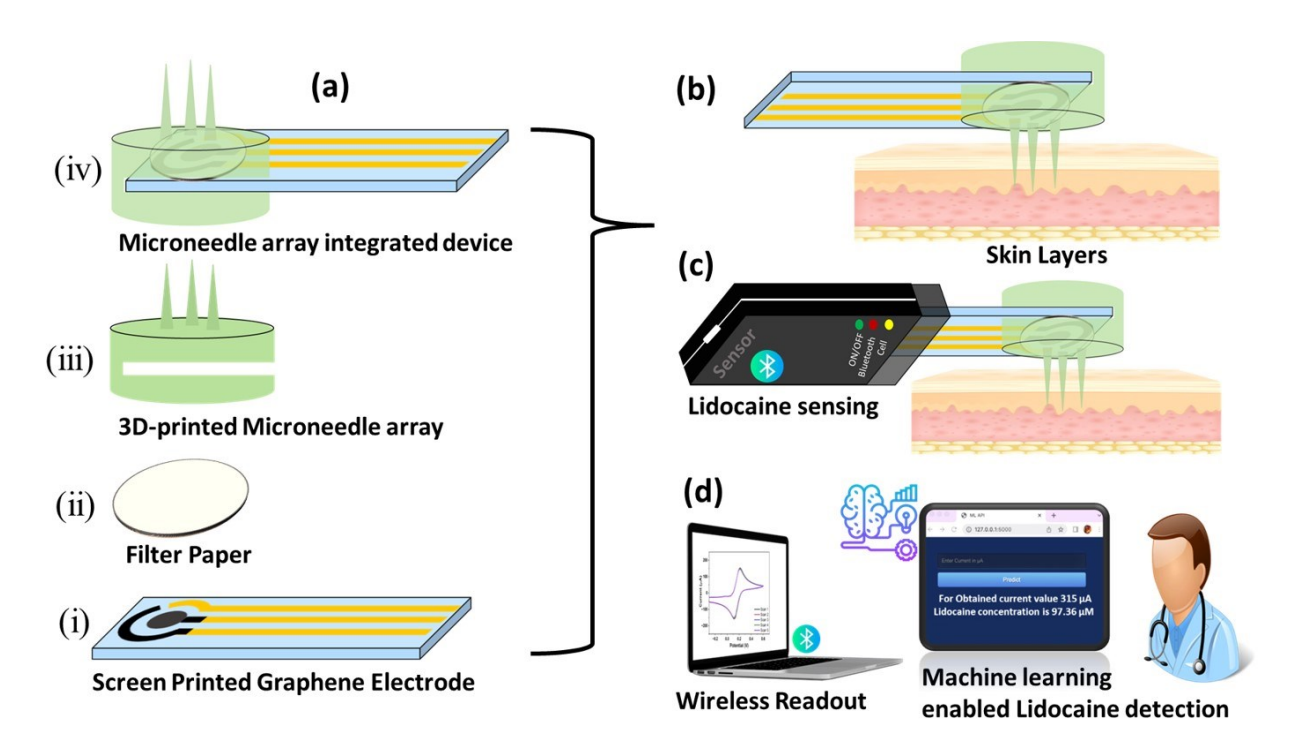


Figure 1. Schematic representation of machine learning-enabled wireless microneedle array integrated screen-printed electrode-based electrochemical point-of-care device for lidocaine detection. (a) Expanded view of components and stepwise assembly process of the microneedle array integrated device. (b) Fully assembled device on skin layer. (c) Fully assembled device connected with wireless sensor. (d) Wireless readout device for further analysis through machine learning enabled linear regression models followed by digital visualization of lidocaine concentration.

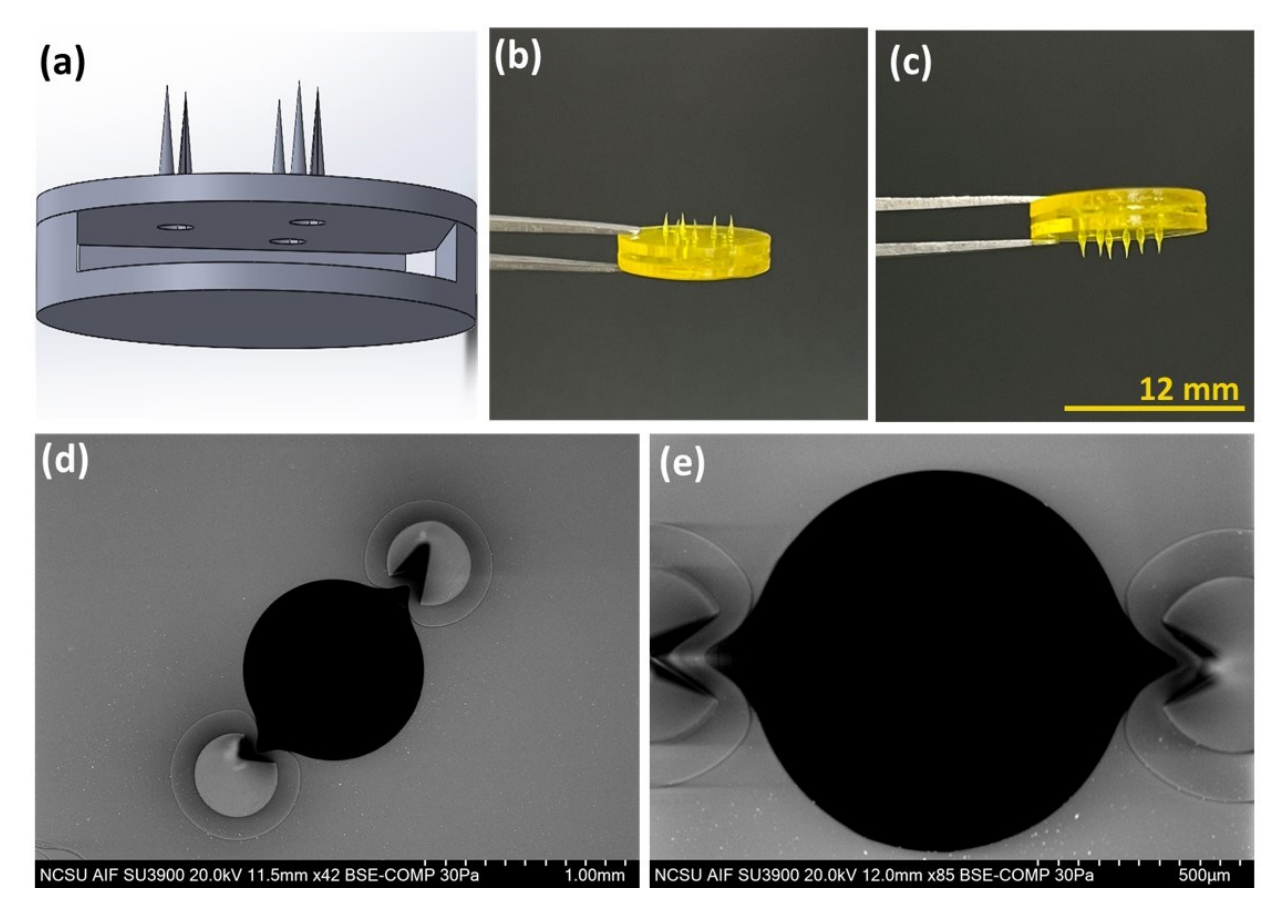


Figure 2. (a) Illustration of the structure of ultra-sharp microneedle array designed using SolidWorks 2016 software. (b and c) Macroscopic image of the 3D-printed microneedle array. (d and e) SEM images of the 3D-printed microneedle array at different angles and magnifications.

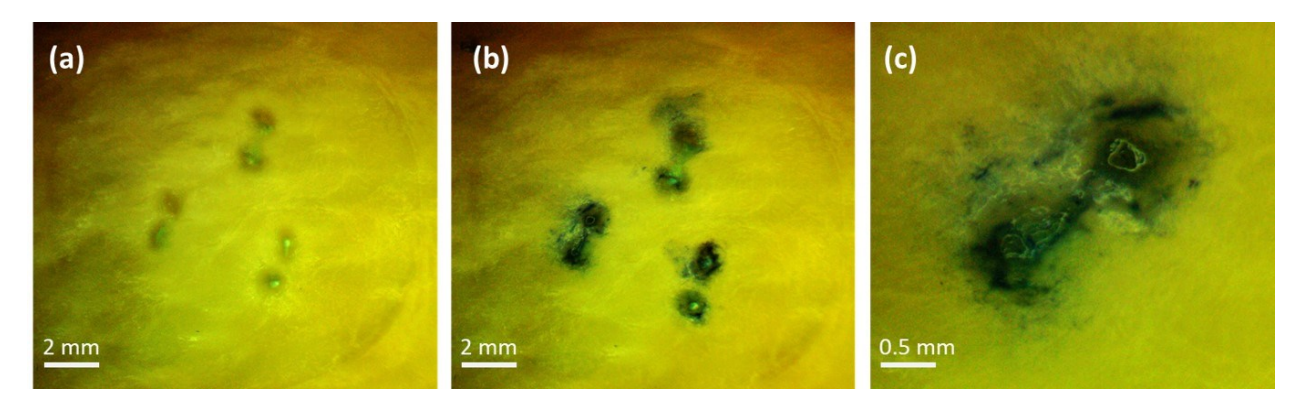


Figure 3. Illustration of skin penetration capability of the 3D-printed microneedle array. (a) Optical images of porcine skin punctured with microneedle array before trypan blue staining. (b and c) After Trypan Blue staining at two different magnifications for better visualization of the pores.

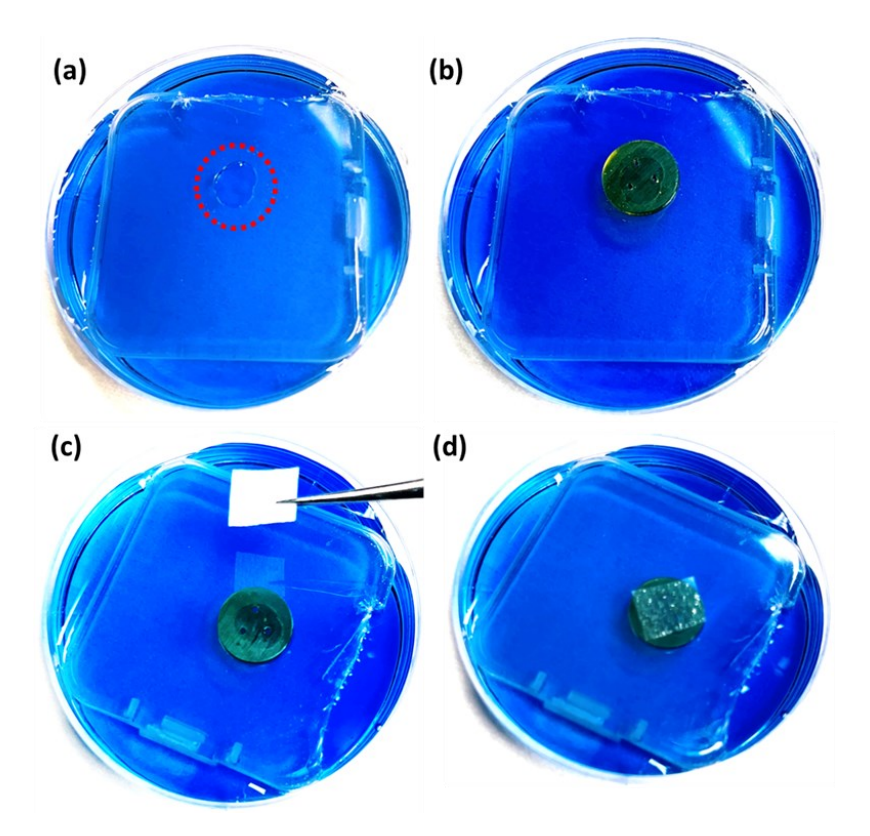


Figure 4. Illustration of fluid extraction capability of the 3D-printed microneedle array. (a) Optical image of a small plastic box equipped with a manually created circular hole (showed in red color circle) placed in a small Petri dish filled with Trypan Blue solution. (b) Placement of the 3D-printed microneedle array onto the manually created circular hole so that the microneedle tips can contact the solution. (c) Placement of the paper substrate on the upper surface of the 3D printed microneedle array. (d) Trypan Blue solution wicked by the paper via the capillarity system.

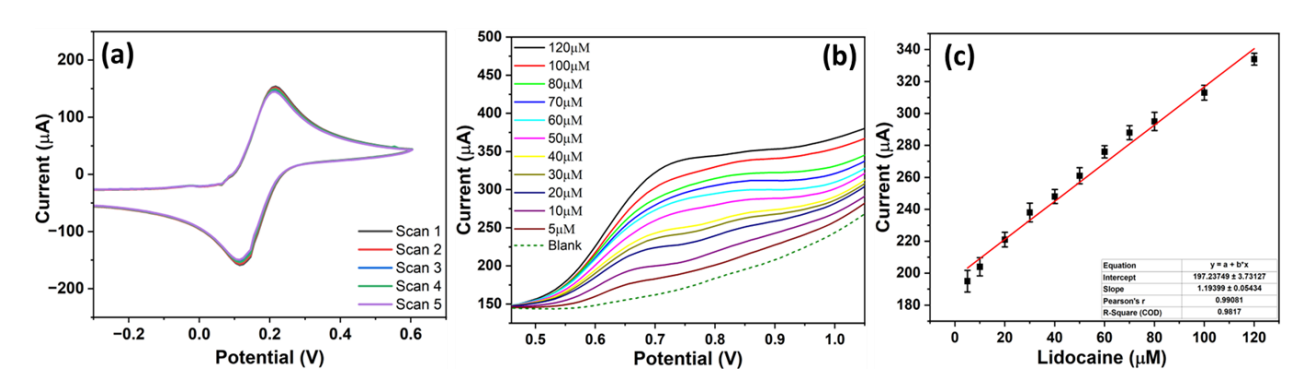


Figure 5. Illustration of electrochemistry, stability and sensing potential of graphene modified screen-printed carbon electrode. (a) Cyclic voltammetry response recorded in freshly prepared 5mM ferricyanide solution at a fixed scan rate of 50 mV/s and room temperature for 5 scans. (b) Square wave voltammetry response of graphene modified screen-printed carbon electrode towards increasing concentrations of lidocaine in freshly prepared phosphate buffered saline electrolyte solution (0.1 M, pH 8) and (c) Respective calibration plots between the recorded peak current values and different concentrations of lidocaine.

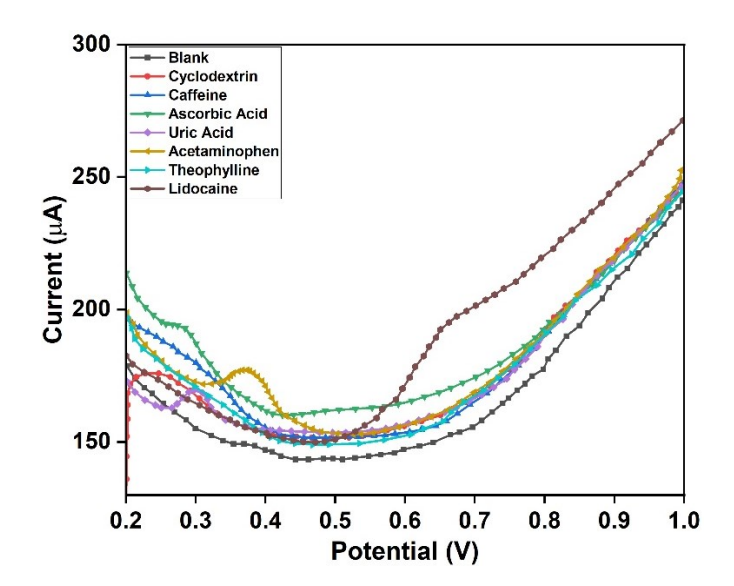


Figure 6. Illustration of the selectivity study through the square wave voltammetry response of the sensing electrode towards various interfering analytes (40 μ M), including cyclodextrin, ascorbic acid, theophylline, acetaminophen, caffeine, uric acid, and lidocaine (10 μ M).

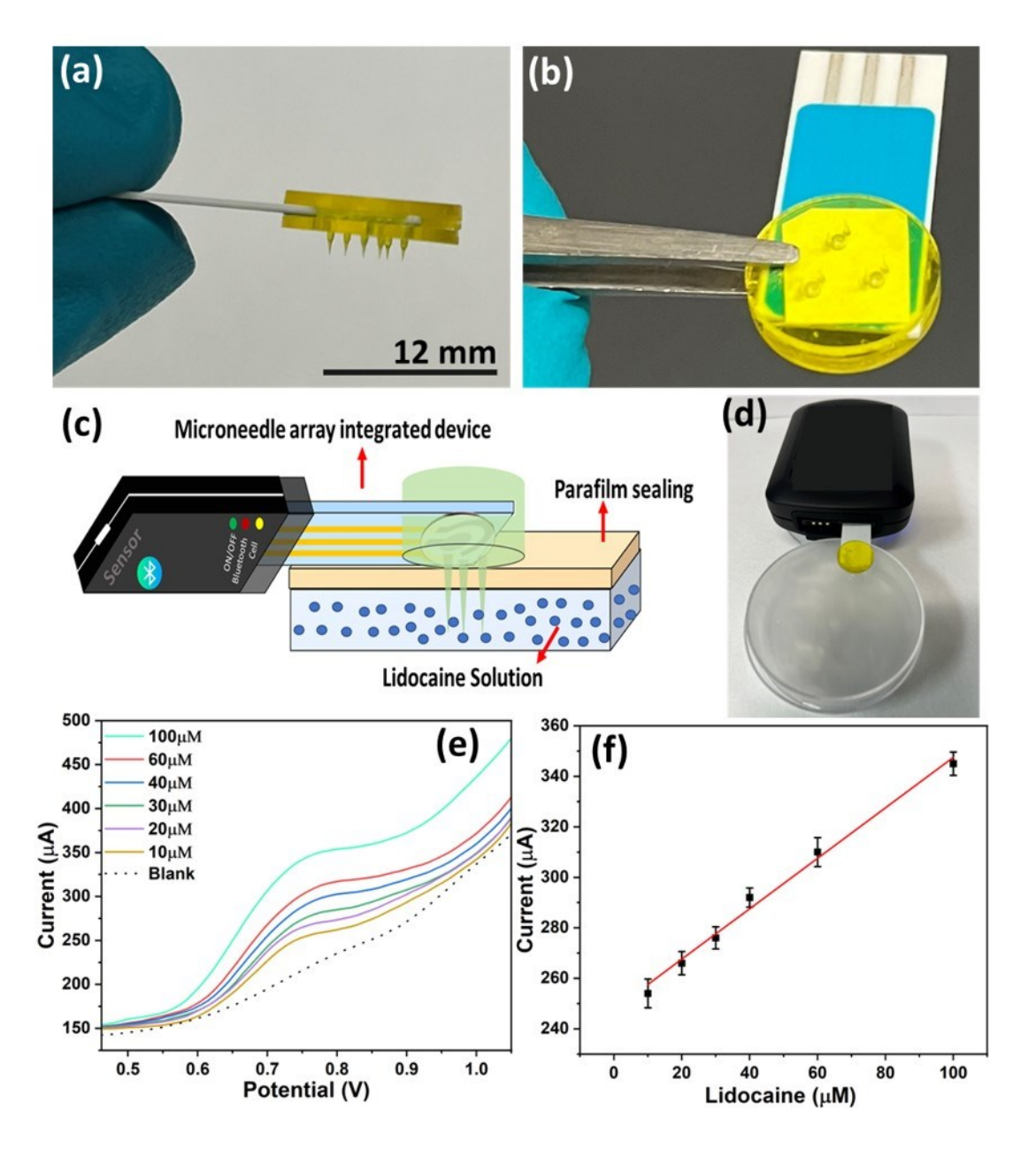


Figure 7. Proof-of-concept demonstration of integrated device. (a and b) Illustration of realistic images of fully assembled device. (c) Schematic diagram and (d) real photograph of experimental setup used for the proof-of concept demonstration. (e) Square wave voltammetry response of the device towards different concentrations of lidocaine spiked in the artificial interstitial fluid. (f) Respective calibration plots between the recorded peak current values and lidocaine concentrations.

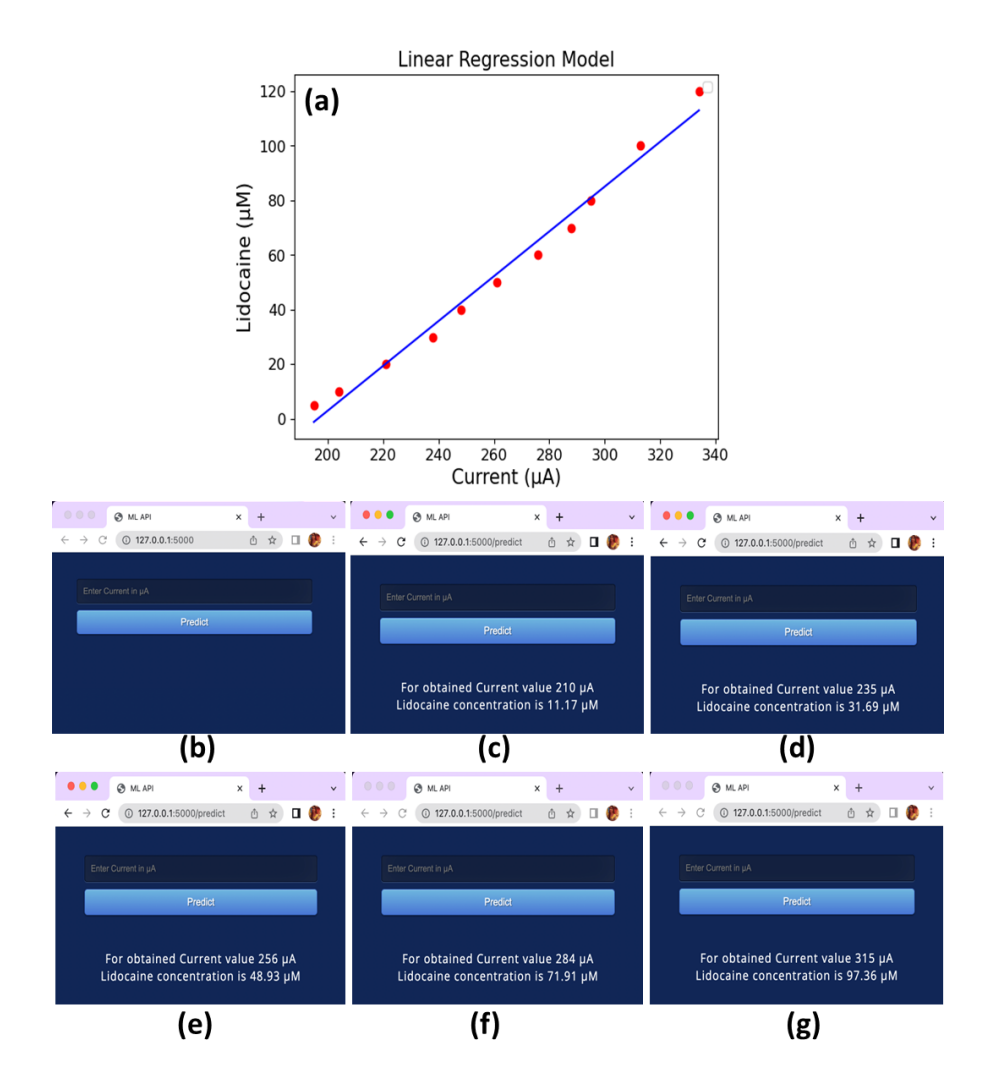


Figure 8. Machine learning enabled detection of lidocaine and digital visualization through web application. (a) Illustration of best-fit line obtained from the developed linear regression model. (b) Screenshot of developed web page user interface. (c-g) Screenshot of web page demonstrating the predicted lidocaine concentration.